



Title	The loop structure of Actinomycete glycoside hydrolase family 5 mannanases governs substrate recognition
Author(s)	Kumagai, Yuya; Yamashita, Keitaro; Tagami, Takayoshi; Uraji, Misugi; Wan, Kun; Okuyama, Masayuki; Yao, Min; Kimura, Atsuo; Hatanaka, Tadashi
Citation	Febs journal, 282(20), 4001-4014 <a href="https://doi.org/10.1111/febs.13401">https://doi.org/10.1111/febs.13401</a>
Issue Date	2015-10
Doc URL	<a href="http://hdl.handle.net/2115/62877">http://hdl.handle.net/2115/62877</a>
Type	article (author version)
File Information	71444(熊谷) .pdf



[Instructions for use](#)

1 The loop structure of *Actinomyces* glycoside hydrolase family 5 mannanases governs  
2 substrate recognition

3

4 Yuya Kumagai<sup>1,2</sup>, Keitaro Yamashita<sup>3</sup>, Takayoshi Tagami<sup>2</sup>, Misugi Uraji<sup>1</sup>, Kun Wan<sup>1</sup>,  
5 Masayuki Okuyama<sup>2</sup>, Min Yao<sup>3,4</sup>, Atsuo Kimura<sup>2</sup>, and Tadashi Hatanaka<sup>1</sup>

6

7 <sup>1</sup>Okayama Prefectural Technology Center for Agriculture, Forestry and Fisheries,  
8 Research Institute for Biological Sciences (RIBS), Okayama 716-1241, Japan

9 <sup>2</sup>Research Faculty of Agriculture, Hokkaido University, Sapporo 060-8589, Japan

10 <sup>3</sup>Graduate School of Life Science and <sup>4</sup>Faculty of Advanced Life Science, Hokkaido  
11 University, Sapporo 060-0810, Japan

12

13 To whom correspondence may be addressed:

14 Tadashi Hatanaka

15 Research Institute for Biological Sciences (RIBS), Okayama, 7549-1 Kibichuo-cho,  
16 Kaga-gun, Okayama 716-1241, Japan

17 Tel: +81 866 56 9452, Fax: +81 866 56 9454; E-mail: hatanaka@bio-ribs.com

18

19 Running title: Substrate Recognition by *Actinomyces* mannanases

20

21 Abbreviations: ABEE, ethyl 4-aminobenzoate; CBM, carbohydrate binding module;  
22 GGM3, 6<sup>I</sup>,6<sup>II</sup>- $\alpha$ -D-galactosyl mannotriose; GGM4, 6<sup>II</sup>,6<sup>III</sup>- $\alpha$ -D-galactosyl  
23 mannotetraose; GGM5, 6<sup>III</sup>,6<sup>IV</sup>- $\alpha$ -D-galactosyl mannopentaose; GH, glycoside  
24 hydrolase family; HPAEC-PAD, high-performance anion-exchange chromatography  
25 with pulsed amperometric detection; LBG, locust bean gum; M1 to M6, mannose to  
26 mannohexaose; StMan, *Streptomyces thermolilacinus* mannanase; StMandC, catalytic  
27 domain of StMan; STMan3dC, chimeric enzyme consisting of 36-246 of StMan and  
28 227-330 of TfMan (*Thermobifida fusca* mannanase); STMan4dC, chimeric enzyme

1 consisting of 36–260 of StMan and 250–330 of TfMan; STMan5dC, chimeric enzyme  
2 consisting of 36–308 of StMan and 288–330 of TfMan; S(S-L7→T-L7)dC, loop7 (276–  
3 283, GPPDQWGD) of StMandC changed to loop7 (256–262, HDHSDGN) of TfMan;  
4 S(S-L8→T-L8)dC, loop8 (308–312, TDPV) of StMandC changed to loop8 (288–293,  
5 GGGVEY) of TfMan; S(S-L7/L8→T-L7/L8)dC, loop7 and loop8 of StMandC changed  
6 to TfMan; TfMan, *Thermobifida fusca* mannanase; TfMandC, catalytic domain of  
7 TfMan; TSMAN3dC, chimeric enzyme consisting of 29–226 of TfMan and 247–349 of  
8 StMan; T(T-L7→S-L7)dC, loop7 of TfMandC changed to loop7 of StMan; T(T-L8→  
9 S-L8)dC, loop8 of TfMandC changed to loop8 of StMan; T(T-L7/L8→S-L7/L8)dC,  
10 loop7 and loop8 of TfMandC changed to loop7 and loop8 of StMan.

11

12 Keywords: mannanase; actinomycete; galactosylmannooligosaccharide; chimeric  
13 enzyme; glycoside hydrolase family 5

1 **Abstract**

2 Endo- $\beta$ -1,4-mannanases from *Streptomyces thermolilacinus* (StMan) and  
3 *Thermobifida fusca* (TfMan) showed different substrate specificities. StMan hydrolyzed  
4 galactosylmannooligosaccharide (GGM5; 6<sup>III</sup>,6<sup>IV</sup>- $\alpha$ -D-galactosyl mannopentaose) to  
5 GGM3 and M2 while TfMan hydrolyzed GGM5 to GGM4 and M1. To determine the  
6 region involved in the substrate specificity, we constructed chimeric enzymes of StMan  
7 and TfMan and evaluated their substrate specificities. Moreover, the crystal structure of  
8 the catalytic domain of StMan (StMandC) and the complex structure of the inactive  
9 mutant StE273AdC with M6 were solved at 1.60 and 1.50 Å resolution, respectively.  
10 Structural comparisons of StMandC and TfMandC lead to the identification of a subsite  
11 around -1 in StMandC which could accommodate a galactose branch. These findings  
12 demonstrate that the two loops (loop7 and loop8) are responsible for substrate  
13 recognition in GH5 actinomycete mannanases. In particular, Trp281 in loop7 of StMan,  
14 which is located in a narrow and deep cleft, plays an important role in its affinity toward  
15 linear substrates. Asp310 in loop8 of StMan specifically bound to the galactosyl unit in  
16 the -1 subsite.

17

1 **Introduction**

2 Plant biomass is an abundant carbon source and important sustainable biomaterial.  
3 The plant cell wall comprises cellulose, hemicelluloses, and lignin. Microbial enzymatic  
4 degradation is a key requirement for the involvement of the carbon cycle in the  
5 utilization of hard biomass [1-3]. Cellulose, a  $\beta$ -1,4-linked glucose polymer, can be  
6 converted to bioenergy [4]. Hemicellulose, a polymer composed of various types of  
7 sugars, also has the potential to be a sustainable biomaterial for bioenergy and bioactive  
8 compounds [5-7]. Mannan is one of the major hemicellulose components that exist as  
9 glucomannan or galactomannan in softwood or bean seeds [8]. Mannan consists of  
10  $\beta$ -1,4-linked mannose polymers which are decorated with  $\alpha$ -1,6-linked galactose  
11 branches. The amount of branched chains is dependent on the species and is also related  
12 to the physical properties of mannan [9-11].

13 For the deconstruction of mannan, cooperative degradation via a series of  
14 glycoside hydrolases [e.g.,  $\beta$ -1,4-mannanase (**EC 3.2.1.78**),  $\beta$ -1,4-mannosidase (**EC**  
15 **3.2.1.25**),  $\alpha$ -galactosidase (**EC 3.2.1.22**)] and accessory enzymes (e.g., carbohydrate  
16 esterases) are necessary [12-14]. Mannanases, a major enzyme group used for mannan  
17 degradation, has been classified into three groups, glycoside hydrolase family (GH) 5, 26,  
18 and 113 (<http://www.cazy.org/>). Among these groups, GH5 mannanase is considered to  
19 primarily function in hemicellulose deconstruction because most GH5 mannanases are  
20 extracellular hydrolases and have carbohydrate binding modules (CBMs) [15, 16]. CBMs  
21 usually bind to insoluble or soluble saccharides with various conformations via a linker  
22 domain to increase the catalytic efficiency of the enzymes [17]. Recently, accessory  
23 enzymes with CBMs have been speculated to be involved in the cooperative  
24 deconstruction of the plant cell wall [18, 19]. The molecular architecture of most GH26  
25 mannanases consists of only a catalytic domain which cannot hydrolyze mannan in the  
26 plant cell wall, while some GH26 mannanases with CBMs do exhibit hydrolysis activity  
27 toward mannan [20], suggesting that target saccharides are differentiated by mannanases  
28 depending on whether they have CBMs or not [21]. Therefore, the analysis of the

1 molecular architecture of these enzymes is important for improving our understanding of  
2 the deconstruction of hemicellulose. The degradation of linear saccharides by catalytic  
3 domains has been extensively studied [22-25]. Some GH5 mannanases exhibit high  
4 activity toward short substrates [26-28]. Specificity toward branched mannan has been  
5 studied in *Streptomyces* sp. SirexAA-E mannanase [29]. However, it is still unclear how  
6 the catalytic domains of these enzymes recognize and degrade linear or branched mannan  
7 structures.

8 We have studied the relationship between the structure and function of GH5  
9 actinomycete mannanases [30-33]. The end-products of locust bean gum (LBG:  
10 galactosyl mannan) degraded by a catalytic domain of mannanase from *Streptomyces*  
11 *thermolilacinus* (StMandC) were mainly M2 and M3, while that from *Thermobifida*  
12 *fusca* (TfMandC) were mainly M1, and M2 [33]. Mannanase activity toward mannan  
13 usually decreases as the degree of modification of branched chain galactoses increases.  
14 Understanding the mechanism of mannanase catalysis of galactosyl-mannan should  
15 provide further insight into mannan degradation, and improve the use of an optimal  
16 combination of mannanase and other hydrolases or accessory enzymes for mannan  
17 degradation.

18 In this study, by using linear mannoooligosaccharides and branched galactosyl  
19 mannoooligosaccharide, we investigated the substrate specificities of StMandC and  
20 TfMandC. Moreover, we investigated the role of two loops (loop7 and loop8) in their  
21 substrate specificity toward linear mannoooligosaccharides and branched galactosyl  
22 mannoooligosaccharides (GGM5) by using StMan, TfMan, their chimeric enzymes, and  
23 mutants. To confirm the kinetic results, we solved the crystal structure of StMandC and a  
24 complex structure of the inactive mutant StE273AdC with M6. Our data demonstrated  
25 the relationship between the structure and substrate specificity of GH5 actinomycete  
26 mannanases.

27

## 28 **Results**

1 *Identification of the region involved in substrate specificity*

2       When StMandC hydrolyzed GGM5, two peaks were detected by HPAEC-PAD  
3 analysis. One peak was determined to be mannobiose (M2) and the remaining  
4 degradation product was identified as GGM3 (Fig. 1A and B). However, when TfMandC  
5 hydrolyzed GGM5, mannose (M1) was detected (Fig. 1B). Mannose residues at the  
6 reducing and non-reducing termini were present in GGM5. Using a labelling agent  
7 (ABEE), we modified the reducing terminus of the sugar to evaluate the mannanase  
8 hydrolysis pattern of GGM5. The hydrolysis product of GGM5-ABEE by TfMandC was  
9 M1-ABEE, indicating that TfMandC hydrolyzed the reducing terminus of GGM5 (Fig.  
10 1C).

11       Four chimeric mannanases (STMan3dC consisting of residues 36–246 of StMan  
12 and 227–330 of TfMan, STMan4dC consisting of 36–260 of StMan and 250–330 of  
13 TfMan, STMan5dC consisting of 36–308 of StMan and 288–330 of TfMan, and  
14 TSMAN3dC consisting of 29–226 of TfMan and 247–349 of StMan) were constructed to  
15 evaluate the GGM5 hydrolysis pattern (Fig. 2A). STMan3dC and STMan4dC  
16 hydrolyzed GGM5 to form GGM4 and M1 and TSMAN3dC produced GGM3 and M2 (Fig.  
17 3A). The C-terminal region (amino acid residues 258–349 in StMan) has been speculated  
18 to determine the substrate specificity of StMan. STMan5dC was significantly less  
19 reactive toward GGM5 compared with the parent enzymes and the three other chimeric  
20 mutants (for example, GGM5 activity of StMandC and STMan5dC were 10.1 and 0.012  
21 U/mg, respectively). STMan5dC exhibited the GGM5-cleavage reactions of two  
22 wild-type enzymes in terms of its GGM5 hydrolysis products (M1, M2, GGM3, and  
23 GGM4), indicating that the GGM5 hydrolysis pattern could be determined by two  
24 regions: the amino acid sequences 258–302 and 303–349 of StMan (Figs. 2A and 3A).  
25 The alignment of these regions of StMandC and TfMandC showed that both regions  
26 contain two single-loop-structures with low sequence identity [loop7: 276–283  
27 (GPPDQWGD) for StMan and 256–262 (HDHSDGN) for TfMan; loop8: 309–312  
28 (TDPV) for StMan and 288–293 (GGGVEY) for TfMan] (Fig. 2B). We then constructed

1 six substitution mutants, of which loop7 and loop8 of StMandC were replaced with those  
2 of TfMandC and vice versa (S(S-L7 → T-L7)dC, S(S-L8 → T-L8)dC, S(S-L7/L8 →  
3 T-L7/L8)dC, T(T-L7 → S-L7)dC, T(T-L8 → S-L8)dC, and T(T-L7/L8 → S-L7/L8)dC; see  
4 Fig. 2C for construction of mutants), and evaluated the GGM5 hydrolysis patterns with  
5 these mutants. S(S-L7 → T-L7)dC, S(S-L7/L8 → T-L7/L8)dC, T(T-L7 → S-L7)dC could not  
6 hydrolyze GGM5. S(S-L8 → T-L8)dC and T(T-L8 → S-L8)dC hydrolyzed GGM5 with  
7 significantly lower activity to produce M1, M2, GGM3, and GGM4 (Fig. 3B). The  
8 GGM5 hydrolysis products of T(T-L7/L8 → S-L7/L8)dC having loop7 and loop8 of  
9 StMan were identical to those of StMan (Fig. 3B). Based on these results, we concluded  
10 the substrate specificity of mannanases is determined by the two loop-structures.

11

#### 12 *Kinetic parameters of StMandC and TfMandC*

13 Both of StMandC and TfMandC displayed no activity on M2 and drastically low  
14 activity on M3, making it impossible to determine the kinetic parameters for these two  
15 substrates. Therefore, the kinetic parameters of mannanases toward  
16 mannoooligosaccharides (M4, M5, and M6) and GGM5 are listed in Table 1. Among these  
17 substrates, both enzymes showed the highest activity toward M6. The  $k_{cat}/K_m$  values  
18 toward M5 and M4 of StMandC were approximately 10- and 100-fold lower than that of  
19 M6. The  $k_{cat}/K_m$  values toward M4 of TfMandC were approximately 100-fold lower than  
20 that of M5 and M6. The  $k_{cat}/K_m$  values of StMandC toward M4, M5, and M6 was 1.6-,  
21 13-, and 2.4-fold lower than those of TfMandC, respectively. In particular, TfMandC had  
22 a 13-fold higher  $k_{cat}$  value toward M5 than that of StMandC. However, both enzymes  
23 were the least active toward GGM5. The values of  $k_{cat}/K_m$  toward GGM5 were very low  
24 compared with linear mannoooligosaccharides. The  $k_{cat}/K_m$  and  $k_{cat}$  of StMandC toward  
25 GGM5 were 13- and 10-fold higher than those of TfMandC, respectively.

26

#### 27 *Crystal structures of StMandC and M6-complexed StE273AdC*



1           The crystal structures of StMandC and its inactive mutant, StE273AdC, with  
2 substrate were solved. The overall structure of StMandC revealed that the protein was  
3 composed of a ( $\beta/\alpha$ )<sub>8</sub>-barrel fold similar to that of other GH5 mannanases belonging to  
4 Clan GH-A (Fig. 4A). StMandC possessed calcium ion-binding site and one residue  
5 (Glu286) has been found as calcium ion-binding residue [31]. From crystal structure of  
6 StMandC, the side chain of Glu286 and Asp283, and main chain of Gly276 and Pro284  
7 were involved in calcium ion-binding in loop7. The structure of StE273AdC in complex  
8 with substrate was successfully determined by soaking with M6 (Fig. 4A). The electron  
9 density map of mannose residues was found at subsites -4 to +3 (Fig. 4B), indicating  
10 various binding patterns of M6 to StE273AdC, since seven subsites (i.e., seven mannose  
11 units) were found by soaking with M6. The subsite -1 was occupied by two moieties of  
12 mannose, an internal moiety in the boat-form conformation B<sub>2,5</sub> and a reducing-terminal  
13 moiety in the skew-boat conformation <sup>1</sup>S<sub>5</sub>, whose equatorial O1 was interacted with  
14 Tyr246 by a 2.72 Å hydrogen bond (Fig. 4C). These conformations represented one of  
15 the structures of the mannose chain [34]. The plus subsites in StMandC consisted of a  
16 hydrophobic cleft, Trp215 at subsite +1, Trp281 at subsite +2, and Trp219 at subsite +3.  
17 Gln217 in loop5 bound to the OH-C(3) of mannose at subsite +2 with a 2.84 Å hydrogen  
18 bond. Binding of OH-C(2) mannose was thought to play a key role in determining the  
19 substrate specificity between mannanases and cellulases [22]. Trp219 and Asn182 bound  
20 to the OH-C(2) of mannose at subsite +2 with a 2.99 and 3.33 Å hydrogen bond,  
21 respectively. These residues created a narrow and deep cleft at the plus subsite side. The  
22 crystal structure of StE273AdC complexed with substrate revealed that the cleft was  
23 suitable for the incorporation of mannose residues containing a twisted glycoside linkage  
24 at subsites -1 and +1. The superimposed model of StMandC and StE273AdC showed  
25 that loop7 of StE273AdC shifted toward the substrate (Fig. 4A and B). Trp281 in loop7  
26 moved into proximity to subsite +2 mannose, which would increase the interaction with  
27 the substrate (Fig. 4D). Thus, we speculated that Trp281 in loop7 plays an important role  
28 in substrate recognition.

1           The superimposed model of StE273AdC with M6 and *T. fusca* KW3 mannanase  
2 with M3 (PDB code: **3MAN**) showed that the mannose main chain was almost coincident  
3 at subsites -3 to -2, and the substrate-binding residues were well conserved, with the  
4 exception of Val263 (3MAN) bound to mannose at subsite -1, which did not correspond  
5 to the StMandC residue (Fig. 5A) [22]. Thr309 in loop8 of StMan, equivalent to Gly260  
6 in 3MAN, was most likely involved in the binding of OH-C(6) mannose at subsite -3  
7 (Fig. 5A). The plus subsites were compared with *T. fusca* KW3 mannanase (PDB code:  
8 **1BQC**) because the structure of 3MAN was lacking loop7 (Fig. 5B). Amino acid residues  
9 in loop4 and loop5 comprising the plus subsites were conserved (Fig. 5B). However,  
10 those of loop7 and loop8 comprising the opposite plus subsites were different: 1BQC had  
11 a wide cleft because of a short loop7 compared with that of StMandC, while Trp281 in  
12 loop7 of StMan constituted a narrow and deep cleft with loop4 and loop5 (Fig. 6).  
13 Additionally, loop7 and loop8 in StMandC generated a space around subsite -1 (Fig. 6B).  
14 It was supposed that this space accommodated the galactose branch, resulting in the  
15 different GGM5 hydrolysis patterns. The crystal structure of StMandC revealed that  
16 Asp310 in loop8 binds to the galactose branch around the -1 subsite.

17

#### 18 *Amino acid residues related to the substrate specificity of mannanases*

19           From the structure of StMandC, we speculated that Trp281 in loop7 and Asp310 in  
20 loop8 were a mannose-main-chain binding residue and galactose-branch-chain binding  
21 residue, respectively. We constructed alanine mutants of Trp281 (StW281AdC) and  
22 Asp310 (StD310AdC). The kinetic parameters for StW281AdC decreased for the  
23 substrates. Their  $k_{\text{cat}}/K_{\text{m}}$  toward linear mannoooligosaccharides (M4–M6) was 7- to  
24 2-fold lower than those of StMandC (Table 1). The  $k_{\text{cat}}/K_{\text{m}}$  of StD310AdC toward GGM5  
25 decreased approximately 5-fold compared with that of StMandC (Table 1).

26

#### 27 **Discussion**

28           Understanding enzymatic properties is essential for determining an enzyme's role

1 in nature. Herein, we found that the substrate specificity of two types of GH5  
2 actinomycete mannanases were related to their loop structures. Namely, a combination of  
3 loop7 and loop8 of StMandC is essential for accommodation of the galactose branch at  
4 the -1 subsite, however the residues critical for determining the substrate specificity  
5 were unclear.

6 The value of  $k_{\text{cat}}$  of StMandC toward GGM5 was the main factor determining the  
7 value of  $k_{\text{cat}}/K_{\text{m}}$ . The value of  $k_{\text{cat}}$  was  $10^2$ – $10^4$ -fold lower compared with those for the  
8 linear substrates. GGM5 is composed of a mannopentaose main chain with two galactose  
9 branches, suggesting that the galactose branches affected the  $k_{\text{cat}}$ . The crystal structure of  
10 GH5 endoglucanase and  $\beta$ -mannosidase revealed that the sugar at subsite -1 was  
11 distorted, and the glycoside linkage between subsites -1 and +1 was twisted [28, 35].  
12 The complex structure of GH26 mannanase with a manooligosaccharide possessing a  
13 galactose branch at the -1 subsite indicated that the galactose residue affected the  
14 mannose chain at the +1 subsite [36]. The complex structure of StE273AdC also revealed  
15 that the glycoside linkage between subsites -1 and +1 was twisted. The distortion of the  
16 sugar at the -1 resulted in a decrease in the distance between the OH-C(6) mannose at  
17 subsite -1 and the OH-C(3) mannose at subsite +1 and a decrease in the catalytic  
18 efficiency toward GGM5. Asp310 in loop8, which could not bind to the mannose main  
19 chain, is located around the -1 subsite. The decrease in  $k_{\text{cat}}/K_{\text{m}}$  toward GGM5 was  
20 primarily related to the decrease in  $k_{\text{cat}}$ . This indicated that Asp310 may assist in the  
21 distortion of the sugar at the -1 subsite by binding the galactose residue. Trp281 in loop7  
22 of StMandC created a narrow cleft at subsite +2, thereby allowing a mannose residue to  
23 bind with a twisted glycoside linkage between subsites -1 and +1. The parameter most  
24 affected by the mutation was the  $k_{\text{cat}}$  toward M4, indicating that Trp281 was an important  
25 residue for the catalytic activity toward the short substrate M4 (Table 1). It was thought  
26 that Trp281 was also necessary for distortion of the sugar at subsite -1. These results  
27 suggest that Trp281 in loop7 is involved in the catalytic activity toward short linear  
28 substrates, while Asp310 in loop8 is specifically involved in the binding of branched

1 substrates. The hydrolysis patterns of GGM5 resulting from these mutants were similar  
2 to that of StMan (i.e., GGM5 was hydrolyzed to GGM3 and M2) (data not shown). Thus,  
3 other residues were also involved in determining the hydrolysis pattern of GGM5.

4 *Streptomyces* sp. SirexAA-E mannanase (SACTE\_2347), which showed 79%  
5 identity with StMandC and possessed loops L1 and L2, corresponding to loop7 and loop8  
6 of StMandC, respectively, hydrolyzed GGM5 to GGM3 and M2 [29]. The crystal  
7 structure of SACTE\_2347 showed the space which could accommodate the galactose  
8 branched around the -1 subsite. Trp281 and Asp310 of StMan were equivalent to Tyr281  
9 and Asp310 of SACTE\_2347, respectively, implying that their possible functions are  
10 short substrate-binding (Tyr281 of SACTE\_2347) and distortion of the sugar at the -1  
11 subsite (Asp310 of SACTE\_2347). Thr309 in loop8, which was conserved in both  
12 enzymes, might be the key residue to determine substrate specificity toward branched  
13 substrates by disturbing the accommodation of galactose branches around the -3 subsite.

14 The value of  $k_{cat}/K_m$  for TfMandC toward GGM5 decreased  $10^5$ -fold compared  
15 with that for M5. For StMandC, the difference in  $k_{cat}/K_m$  between GGM5 and M5 was  
16  $10^3$ -fold. From analysis of the hydrolysis products of GGM5, it was determined that  
17 TfMandC could accommodate the galactose branches in the vicinity of subsites -3 and  
18 -2, while StMandC accommodated galactose branches around subsites -2 and -1. When  
19 using M5 as a substrate, both TfMandC and StMandC remove M1 and M2 from M5 to a  
20 similar amount (Fig. 7). However, the two enzymes had different reactivities toward  
21 GGM5 (Fig. 1). Therefore, the decrease in  $k_{cat}/K_m$  for TfMandC and StMandC toward  
22 GGM5 was related to the steric hindrance created by the accommodation of the galactose  
23 branches. Around subsite -2, loop2 and loop3 could accommodate the galactose branch  
24 (Fig. 5). The putative galactose binding residues between StMandC and TfMandC appear  
25 to be conserved: Arg108 in loop2, and Thr139 and Asp144 in loop3 of StMandC  
26 correspond to Arg58 in loop2, Thr89 and Gln94 in loop3 of TfMandC. Around the -3  
27 subsite, the complex structure of StMandC with M6 showed a 2.7 Å hydrogen bond  
28 between Thr309 and the OH-C(6) of mannose at subsite -3. Therefore, Thr309 should

1 inhibit the accommodation of the galactose branch at the -3 subsite, leading to the  
2 substrate specificity of mannanases. At the -1 subsite, Val263 in loop8 of TfMandC  
3 would fill the space [22] (Fig. 6C). Loop8 was necessary for the substrate specificity of  
4 TfMan-type enzymes because the accommodation of a galactose branch at the -3 subsite  
5 would be attributed to loop8. We assumed that the substrate specificity of the loop8  
6 substitution mutant S(S-L8→T-L8)dC changed to a TfMandC-type, i.e., galactose  
7 branches were accommodated at subsites -3 and -2. However, S(S-L8→T-L8)dC  
8 displayed less hydrolytic reaction: GGM5 to GGM4 and M1. Additionally, the loop8  
9 substitution mutant T(T-L8→S-L8)dC also could not hydrolyze GGM5 to GGM3 and  
10 M2, suggesting that loop7 contained important residues for substrate specificity.  
11 Therefore, we speculated that the difference in the accommodation of mannose residues  
12 at the plus subsites would be directly related to the enzyme's substrate specificity.

13         The synergistic degradation of hemicelluloses has been proposed to be carried out  
14 by GH5 and GH26 mannanases [21]. The genome of *Actinomycete* sp. contains both GH5  
15 and GH26 mannanase genes. Most GH5 mannanases in *Actinomycetes* have  
16 loop-structures similar to those of StMan or TfMan (Fig. 8). Interestingly, several species  
17 such as *Streptomyces coelicolor* A3(2) and *Streptomyces scabiei* 87.22 possess more than  
18 two kinds of GH5 mannanase genes similar to those of StMan and TfMan (Fig. 8).  
19 SACTE\_2347 was classified as a StMan-type enzyme, supporting the close relationship  
20 between the sequence alignment and the function of enzymes. The end-products from  
21 LBG by these enzymes were mainly M2 [29, 33].  $\beta$ -1,4-Mannosidases from GH1 and  
22 GH2 catalyzed further hydrolysis of M2, and some GH5 mannanases could hydrolyze  
23 M2 [26, 27]. GH5  $\beta$ -1,4-mannosidase from *Actinomycete* sp. has not been found,  
24 however it is possible to hydrolyze mannan to mannose by symbiotic degradation among  
25 GH5 mannanases. A combination of GH5 mannanases would have the potential to act  
26 synergistically to deconstruct lignocellulosic materials.

27         In conclusion, this study highlights the different enzyme properties of GH5  
28 mannanases from *Actinomycetes* sp. Both loop7 and loop8 are key regions which

1 determine substrate specificity. StMan-loops can contribute to the hydrolysis of a  
2 mannose chain decorated with a galactose branch around the -1 subsite, while  
3 TfMan-loops show high activity toward linear mannan. The alignment shows that the  
4 many characteristics of mannanases are conserved in *Actinomycetes* sp.

5

## 6 **Materials and methods**

### 7 *Construction, expression, and purification of Actinomycete mannanases*

8 To evaluate the region involved in mannanase substrate specificity, we used  
9 expression plasmids encoding the catalytic domains of StMan (StMandC) and TfMan  
10 (TfMandC) and chimeric enzymes combining StMandC and TfMandC (STMan3dC and  
11 TSMan3dC) [30]. The other chimeric enzymes (STMan4dC and STMan5dC) were  
12 prepared using the Repeat-length-Independent Broad-Spectrum (RIBS) DNA shuffling  
13 method described in the following section. The recombinant proteins were expressed in  
14 *Escherichia coli* BL21-Gold (DE3) cells (Agilent Technologies, Palo Alto, CA, USA)  
15 harboring the pET28a construct (mannanase). The recombinant proteins were purified  
16 from cells as previously described [31] and concentrated using a 10,000-MW cutoff  
17 Amicon<sup>®</sup> ultra membrane (Millipore, Billerica, MA, USA) for use in subsequent  
18 experiments. The purities of the recombinant proteins were confirmed by using  
19 SDS-PAGE [37]. The protein concentrations were determined by the Bradford method  
20 [38] using BSA as the standard.

21

### 22 *Preparation of chimeric enzymes using the RIBS shuffling system*

23 Chimeric enzymes were prepared using the RIBS *in vivo* DNA shuffling system,  
24 which is an improved method of chimera genesis based on highly frequent deletion  
25 formation using the *E. coli* *ssb-3* strain [39]. The parental mannanase genes, gentamicin  
26 resistance gene ( $Gm^r$ ) and *E. coli* *rpsL*<sup>+</sup> gene [streptomycin-sensitive ( $Sm^s$ )], were  
27 tandemly cloned into the *Nde*I-*Hind*III sites of pET28a. The rank order of these genes  
28 was *stman-Gm<sup>r</sup>-E.coli rpsL<sup>+</sup>-tfman*, and then *E. coli* MK1019 [*ssb-3 rpsL* ( $Sm^r$ )]

1 harboring pET28a (StMan/Gm<sup>r</sup>-*rpsL*/TfMan) was obtained. Thirty transformants were  
2 cultured overnight in Luria Broth (LB) medium containing 50 µg/mL chloramphenicol  
3 and each culture was spread and then cultivated on LB plates containing 50 µg/mL  
4 chloramphenicol and 50 µg/mL streptomycin. Plasmids containing chimeric mannanase  
5 (*c-man*) genes were isolated from 80 colonies. A total of 10 clones with different *c-man*  
6 genes were obtained. The catalytic domain of the enzymes was produced by PCR using  
7 a previously reported method [39]. Each chimeric construct was named based on  
8 recombination positions from the N-terminus of StMan. For example, chimera1-Man  
9 (*c1-man*) was designated as ST-C85. Among the *c-man* genes, the catalytic domain  
10 mutants of ST-C258dC and ST-C302dC, which were designated STMan4dC and  
11 STMan5dC, respectively were used in this study.

12

### 13 *Preparation of mutant enzymes*

14 To evaluate the effects of loop-structure on substrate specificity, we generated  
15 loop7 and loop8 substitution mutants (S(S-L7→T-L7)dC, S(S-L8→T-L8)dC, S(S-L7/L8  
16 →T-L7/L8)dC, T(T-L7→S-L7)dC, T(T-L8→S-L8)dC, and T(T-L7/L8→S-L7/L8)dC) by  
17 PCR, restriction enzyme digestion, and ligation. PCR was performed in the following  
18 two conditions: 1) PCR was performed to substitute the amino acid residues in the loop  
19 with a set of primers (S(S-L7→T-L7)dC, StL7Fw1 and StCDRe; S(S-L8→T-L8)dC,  
20 StFw and StL8Re1, and StL8Fw1 and StCDRe); and 2) PCR was performed to insert the  
21 restriction enzyme site for the digestion and ligation of mannanase gene fragments into  
22 pET28a using a set of primers (S(S-L7→T-L7)dC, StFw and StL7Re1; StL7Fw2 and  
23 StCDRe; and S(S-L8→T-L8)dC, StFw and StL8Re2; StL8Fw2 and StCDRe) (Table S1).  
24 The primer sets used to construct the loop-substitution mutants for TfMandC using a  
25 previously reported procedure are listed in Table S1 [30]. The mutant genes  
26 (StW281AdC, StD310AdC, and inactive mutant StE273AdC) were generated by PCR  
27 using site-directed mutagenesis (Prime Star GXL DNA polymerase kit; Takara Bio Inc.)  
28 with the following sets of primers (StW281A-S:

1 5'-CGACCAGGCGGGCGACCCGGACGAGGAC-3' and StW281A-AS:  
2 5'-GGTCGCCCGCCTGGTCGGGCGGCCCGCC-3'; and StD310A-S:  
3 5'-AACACCGCCCCCGTCCTCGACCTGGCG-3' and StD310A-AS:  
4 5'-GACGGGGGCGGTGTTCCCGCTCCACGA-3'; StE273A-S: 5'-  
5 ATCGGGGGCGTTTCGGCGGGCCCGCCCGAC-3' and StE273A-AS: 5'-  
6 GCCGAACGCCCCGATGACCAGCGGCAG-3') (the underline shows the position  
7 changed for alanine) using pET28a-StMandC as a template.  
8

### 9 *Mannanase activity assay*

10 Mannanase activity was determined at 40°C for 10 min in a reaction mixture (0.1  
11 mL) containing an appropriate amount of enzyme, 1% (w/v) LBG, 1 mM CaCl<sub>2</sub>, and 50  
12 mM piperazine-*N,N'*-bis-(2-ethanesulfonic acid) PIPES (pH 7.0) [30, 33]. The amount  
13 of reducing sugars produced by the reaction was determined using the  
14 3,5-dinitrosalicylic acid method [40]. One unit of mannanase activity was defined as the  
15 amount of enzyme that liberates reducing sugars equivalent to 1.0 μmol mannose per  
16 min. All activity assays were performed in triplicate.  
17

### 18 *Evaluation of GGM5 hydrolysis patterns*

19 GGM5 (Megazyme International Ireland Ltd., Bray, Ireland) was derivatized with  
20 ethyl 4-aminobenzoate (ABEE) [41]. GGM5-ABEE was hydrolyzed by StMandC and  
21 TfMandC, and degradation products were analyzed using an HPLC equipped with a C18  
22 column (Cadenza CD-C18, 150 x 4.6 mm, Imtakt Corp., Kyoto, Japan). The samples  
23 were eluted using the following gradient with a flow rate of 1.0 mL/min: 20%  
24 acetonitrile for 0–2 min, a linear gradient to 50% acetonitrile for 2–15 min, and 50%  
25 acetonitrile for 15–20 min. The eluted sugars were detected by UV absorption at 305 nm.  
26

### 27 *Evaluation of the kinetic parameters of mannanases*



1           The kinetic parameters of StMandC, TfMandC, StW281AdC, and StD310AdC  
2 toward mannoooligosaccharides (Megazyme International Ireland Ltd., Bray, Ireland)  
3 were determined using a stopped-assay method involving high-performance  
4 anion-exchange chromatography with pulsed amperometric detection (HPAEC-PAD)  
5 (Dionex, Sunnyvale, CA, USA). A Carbowac PA1 column (4 × 250 mm) (Dionex) with  
6 an isocratic flow of 100 mM NaOH was used for separation. Assay conditions were  
7 0.02–8 mM M4, 0.04–6 mM M5, 0.04–2 mM M6, and 1–50 mM GGM5 with an  
8 appropriate amount of enzymes. Aliquots were withdrawn at four time points during the  
9 5–60 min incubation time, and the reactions were terminated by boiling. The formed  
10 hydrolysis products of GGM5 were determined by HPAEC-PAD. Kinetics for M4–M6  
11 were determined by following the decrease of substrate after hydrolysis because several  
12 products were formed. The  $k_{\text{cat}}$  and  $K_{\text{m}}$  values were determined by relationship between  
13 substrate concentrations and initial hydrolytic velocities using Origin Software  
14 (Lightstone Corp., Tokyo, Japan).

15

#### 16 *Crystallization and data collection of StMandC and StE273AdC with M6*

17           Crystallization was performed using the hanging-drop vapor diffusion method at  
18 20°C. StMandC and StE273AdC were concentrated to 10 mg/ml in 0.1 M Tris-HCl, pH  
19 7.0. The crystallization condition used was 1.1 M sodium malonate (pH 7.0), 0.1 M  
20 HEPES (pH 7.0), and 0.5% (v/v) Jeffamine<sup>®</sup> ED-2001 (pH 7.0). Glycerol was used at a  
21 concentration of 25% as the cryoprotectant. The structure of StE273AdC in complex  
22 with substrate was determined by soaking with M6. X-ray diffraction data of the  
23 StMandC crystal was collected on beamline BL44XU at SPring-8 (Hyogo, Japan) at a  
24 wavelength of 1.0000 Å using MX255HE CCD detector (Rayonix, USA). The X-ray  
25 diffraction data of the StE273AdC crystal was collected on beamline NE3A at the Photon  
26 Factory Advanced Ring, KEK (Tsukuba, Japan) at a wavelength of 1.0000 Å using the  
27 Q270 CCD detector (ADSC, USA). Both diffraction datasets were collected from single  
28 crystals under a stream of nitrogen at 100 K. The diffraction data sets were indexed,

1 integrated, and scaled with *XDS* [42]. The StMandC crystal belonged to the  $P2_12_12_1$   
2 space group with the cell dimensions  $a = 65.86 \text{ \AA}$ ,  $b = 100.85 \text{ \AA}$ , and  $c = 105.24 \text{ \AA}$  and  
3 diffracted to  $1.60 \text{ \AA}$  resolution, and the StE273AdC crystal belonged to the  $P2_12_12_1$   
4 space group with the cell dimensions  $a = 65.71 \text{ \AA}$ ,  $b = 100.71 \text{ \AA}$ , and  $c = 104.74 \text{ \AA}$  and  
5 diffracted to  $1.50 \text{ \AA}$  resolution. The StMandC structure was determined by the molecular  
6 replacement method with *phenix.automr* [43, 44] using **1BQC** (Protein Data Bank code  
7 of *Thermobifida fusca* KW3 mannanase) as a search model. Two molecules are present in  
8 the asymmetric unit. The resultant model was automatically rebuilt by *ARP/wARP* [45]  
9 using the calculated phases. The refinement was converged by several cycles of manual  
10 model corrections with *Coot* [46] and refinement using *phenix.refine* [47]. The  
11 StE273AdC structure was determined by rigid body refinement of the StMandC structure,  
12 followed by several cycles of manual model corrections with *Coot* [46] and refinement  
13 using *phenix.refine* [47]. Ramachandran plot analysis was performed using *MolProbity*  
14 [48]. Coordinates and structure factors have been deposited in the Protein Data Bank  
15 under codes **3WSU** and **4Y7E**. Data processing and refinement statistics are given in  
16 Table 2. The graphical representations were prepared using *PyMOL* (DeLano Scientific;  
17 The PyMOL Molecular Graphics System, Version 1.5.0.4 Schrödinger, LLC.) and  
18 *MolSoft* [49].

19

## 20 **References**

- 21 1. Pauly M & Keegstra K (2008) Cell-wall carbohydrates and their modification as a  
22 resource for biofuels. *Plant J* **54**, 559–568.
- 23 2. Demirbas MF (2009) Biorefineries for biofuel upgrading: a critical review. *Appl*  
24 *Energy* **86**, S151–S161.
- 25 3. Peralta-Yahya PP, Zhang F, del Cardayre SB & Keasling JD (2012) Microbial  
26 engineering for the production of advanced biofuels. *Nature* **488**, 320–328.
- 27 4. Sticklen MB (2008) Plant genetic engineering for biofuel production: towards  
28 affordable cellulosic ethanol. *Nat Rev Genet* **9**, 433–443.

- 1 5. Olsson L & Hahn-Hagerdal B (1996) Fermentation of lignocellulosic hydrolysates  
2 for ethanol production. *Enzyme Microb Technol* **18**, 312–331.
- 3 6. Himmel ME, Ding SY, Johnson DK, Adney WS, Nimlos MR, Brady JW & Foust TD  
4 (2007) Biomass recalcitrance: engineering plants and enzymes for biofuels production.  
5 *Science* **315**, 804–807.
- 6 7. Scheller HV & Ulvskov P (2010) Hemicelluloses. *Annu Rev Plant Biol* **61**, 263–289.
- 7 8. Moreira LR & Filho EX (2008) An overview of mannan structure and  
8 mannan-degrading enzyme systems. *Appl Microbiol Biotechnol* **79**, 165–178.
- 9 9. Bulpin PV, Gidley MJ, Jeffcoat R & Underwood DR (1990) Development of a  
10 biotechnological process for the modification of galactomannan polymers with plant  
11 alpha-galactosidase. *Carbohydr Polym* **12**, 155–168.
- 12 10. Daas PJ, Schols HA & de Jongh HH (2000) On the galactosyl distribution of  
13 commercial galactomannans. *Carbohydr Res* **329**, 609–619.
- 14 11. Rinaudo M (2004) Role of substituents on the properties of some polysaccharides.  
15 *Biomacromolecules* **5**, 1155–1165.
- 16 12. Clarke JH, Davidson K, Rixon JE, Halstead JR, Fransen MP, Gilbert HJ &  
17 Hazlewood GP (2000) A comparison of enzyme-aided bleaching of softwood paper pulp  
18 using combinations of xylanase, mannanase and  $\alpha$ -galactosidase. *Appl Microbiol*  
19 *Biotechnol* **53**, 661–667.
- 20 13. Puchart V & Biely P (2005) Glycosylation of internal sugar residues of  
21 oligosaccharides catalyzed by  $\alpha$ -galactosidase from *Aspergillus fumigatus*. *Biochim*  
22 *Biophys Acta* **1726**, 206–216.
- 23 14. Dhawan S & Kaur J (2007) Microbial mannanases: an overview of production and  
24 applications. *Crit Rev Biotechnol* **27**, 197–216.
- 25 15. Boraston AB, Bolam DN, Gilbert HJ & Davies GJ (2004) Carbohydrate-binding  
26 modules: fine-tuning polysaccharide recognition. *Biochem J* **382**, 769–781.
- 27 16. Gilbert HJ, Knox JP & Boraston AB (2013) Advances in understanding the  
28 molecular basis of plant cell wall polysaccharide recognition by carbohydrate-binding

- 1 modules. *Curr Opin Struct Biol* **23**, 669-677.
- 2 17. da Silva VM, Colussi F, Neto MO, Braz ASK, Squina FM, Oliveira CL & Garcia W  
3 (2014) Modular hyperthermostable bacterial endo-beta-1,4-mannanase: molecular shape,  
4 flexibility and temperature-dependent conformational changes. *PLoS One* **9(3)**, e92996.
- 5 18. Montanier C, Money VA, Pires VM, Flint JE, Pinheiro BA, Goyal A, Prates JA,  
6 Izumi A, Stålbrand H, Morland C, Cartmell A, Kolenova K, Topalas E, Dodson EJ,  
7 Bolam DN, Davies GJ, Fontes CM & Gilbert HJ (2009) The active site of a carbohydrate  
8 esterase displays divergent catalytic and noncatalytic binding functions. *PLoS Biol* **7**,  
9 e71.
- 10 19. Zhang X, Rogowski A, Zhao L, Hahn MG, Avci U, Knox JP & Gilbert HJ (2014)  
11 Understanding how the complex molecular architecture of mannan degrading hydrolases  
12 contributes to plant cell wall degradation. *J Biol Chem* **289**, 2002–2012.
- 13 20. Couturier M, Roussel A, Rosengre A, Leone P, Stålbrand H & Berrin JG (2013)  
14 Structural and biochemical analyses of glycoside hydrolase families 5 and 26  
15  $\beta$ -(1,4)-mannanases from *Podospora anserina* reveal differences upon  
16 manno-oligosaccharide catalysis. *J Biol Chem* **288**, 14624–14635.
- 17 21. Hogg D, Pell G, Dupree P, Goubet F, Martin-Orue SM, Armand S & Gilbert HJ  
18 (2003) The modular architecture of *Cellvibrio japonicus* mannanases in glycoside  
19 hydrolase families 5 and 26 points to differences in their role in mannan degradation.  
20 *Biochem J* **371**, 1027–1043.
- 21 22. Hilge M, Gloor SM, Rypniewski W, Sauer O, Heightman TD, Zimmermann W,  
22 Winterhalter K & Piontek K (1998) High-resolution native and complex structures of  
23 thermostable beta-mannanase from *Thermomonospora fusca* – substrate specificity in  
24 glycosyl hydrolase family 5. *Structure* **6**, 1433–1444.
- 25 23. Larsson AM, Anderson L, Xu B, Muñoz IG, Usón I, Janson JC, Stålbrand H &  
26 Ståhlberg J (2006) Three-dimensional crystal structure and enzymatic characterization of  
27  $\beta$ -mannanase Man5A from blue mussel *Mytilus edulis*. *J Mol Biol* **357**, 1500–1510.

- 1 24. Tailford LE, Ducros VM, Flint JE, Roberts SM, Morland C, Zechel DL, Smith N,  
2 Bjørnvad ME, Borchert TV, Wilson KS, Davies GJ & Gilbert HJ (2009) Understanding  
3 how diverse  $\beta$ -mannanases recognize heterogeneous substrates. *Biochemistry* **48**, 7009–  
4 7018.
- 5 25. Santos CR, Paiva JH, Meza AN, Cota J, Alvarez TM, Ruller R, Prade RA, Squina  
6 FM & Murakami MT (2012) Molecular insights into substrate specificity and thermal  
7 stability of a bacterial GH5-CBM27 endo-1,4- $\beta$ -D mannanase. *J Struct Biol* **177**, 469–  
8 476.
- 9 26. Dias FM, Vincent F, Pell G, Prates JA, Centeno MS, Tailford LE, Ferreira LM,  
10 Fontes CM, Davies GJ & Gilbert HJ (2004) Insights into the molecular determinants of  
11 substrate specificity in glycoside hydrolase family 5 revealed by the crystal structure and  
12 kinetics of *Cellvibrio mixtus* mannosidase 5A. *J Biol Chem* **279**, 25517–25526.
- 13 27. Goncalves AM, Silva CS, Madeira TI, Coelho R, de Sanctis D, San Romão MV &  
14 Bento I (2012) Endo- $\beta$ -D-1,4-mannanase from *Chrysonilia sitophila* displays a novel  
15 loop arrangement for substrate selectivity. *Acta Crystallogr D Biol Crystallogr* **68**, 1468–  
16 1478.
- 17 28. Zhou, P, Liu Y, Yan Q, Chen Z, Qin Z & Jiang Z (2014) Structural insights into the  
18 substrate specificity and transglycosylation activity of a fungal glycoside hydrolase  
19 family 5 beta-mannosidase. *Acta Crystallogr D Biol Crystallogr* **70**, 2970–2982.
- 20 29. Takasuka TE, Acheson JF, Bianchetti CM, Prom BM, Bergeman LF, Book AJ,  
21 Currie CR & Fox BG (2014) Biochemical properties and atomic resolution structure of a  
22 proteolytically processed  $\beta$ -mannanase from cellulolytic *Streptomyces* sp. SirexAA-E.  
23 *PLoS One* **9(4)**, e94166.
- 24 30. Kumagai Y, Usuki H, Yamamoto Y, Yamasato A, Arima J, Mukaihara T & Hatanaka  
25 T (2011) Characterization of calcium ion sensitive region for beta-mannanase from  
26 *Streptomyces thermolilacinus*. *Biochim Biophys Acta* **1814**, 1127–1133.
- 27 31. Kumagai Y, Kawakami K, Mukaihara T, Kimura M & Hatanaka T (2012) The  
28 structural analysis and the role of calcium binding site for thermal stability in mannanase.

- 1 *Biochimie* **94**, 2783–2790.
- 2 32. Kumagai Y, Kawakami K, Uraji M & Hatanaka T (2013) Binding of bivalent ions  
3 to actinomycete mannanase is accompanied by conformational change and is a key factor  
4 in its thermal stability. *Biochim Biophys Acta* **1834**, 301–307.
- 5 33. Kumagai Y, Kawakami K, Uraji M & Hatanaka T (2013) Effect of the binding of  
6 bivalent ion to the calcium-binding site responsible for the thermal stability of  
7 actinomycete mannanase: potential use in production of functional  
8 mannoooligosaccharides. *J Mol Catal B Enzym* **94**, 63–68.
- 9 34. Ardevol A, Biarnes X, Planas A & Rovira C (2010) The conformational free-energy  
10 landscape of beta-D-mannopyranose: Evidence for a  ${}^1S_5 \rightarrow B_{2,5} \rightarrow {}^0S_2$  catalytic itinerary  
11 in beta-mannosidases. *J Am Chem Soc* **132**, 16058–16065.
- 12 35. Kim HW & Ishikawa K (2011) Functional analysis of hyperthermophilic  
13 endocellulase from *Pyrococcus horikoshii* by crystallographic snapshots. *Biochem J* **437**,  
14 223–230.
- 15 36. Cartmell A, Topakas E, Ducros VM, Suits MD, Davies GJ & Gilbert HJ (2008) The  
16 *Cellvibrio japonicus* mannanase CjMan26C displays a unique exo-mode of action that is  
17 conferred by subtle changes to the distal region of the active site. *J Biol Chem* **283**,  
18 34403–34413.
- 19 37. Porzio MA & Pearson AM (1977) Improved resolution of myofibrillar proteins with  
20 sodium dodecyl sulfate-polyacrylamide gel electrophoresis. *Biochim Biophys Acta* **490**,  
21 27–34.
- 22 38. Bradford MM (1976) A rapid and sensitive method for the quantitation of  
23 microgram quantities of protein utilizing the principle of protein–dye binding. *Anal*  
24 *Biochem* **72**, 248–254.
- 25 39. Mori K, Mukaihara T, Uesugi Y, Iwabuchi M & Hatanaka T (2005)  
26 Repeat-Length-Independent Broad-Spectrum Shuffling, a novel method of generating a  
27 random chimera library *in vivo*. *Appl Environ Microbiol* **71**, 754–760.
- 28 40. Miller GL (1959) Use of dinitrosalicylic acid reagent for determination of reducing

- 1 sugar. *Anal Chem* **31**, 426–428.
- 2 41. Wang WT, LeDonne NC, Ackerman B & Sweeley CC (1984) Structural  
3 characterization of oligosaccharides by high-performance liquid chromatography,  
4 fast-atom bombardment-mass spectrometry, and exoglycosidase digestion. *Anal Biochem*  
5 **141**, 366–381.
- 6 42. Kabsch W (2010) XDS. *Acta Crystallogr D Biol Crystallogr* **66**, 125–132.
- 7 43. Adams PD, Afonine PV, Bunkóczi G, Chen VB, Davis IW, Echols N, Headd JJ,  
8 Hung LW, Kapral GJ, Grosse-Kunstleve RW, McCoy AJ, Moriarty NW, Oeffner R, Read  
9 RJ, Richardson DC, Richardson JS, Terwilliger TC & Zwart PH (2010) PHENIX: a  
10 comprehensive Python-based system for macromolecular structure solution. *Acta*  
11 *Crystallogr D Biol Crystallogr* **66**, 213–221.
- 12 44. McCoy AJ, Grosse-Kunstleve RW, Adams PD, Winn MD, Storoni LC & Read RJ  
13 (2007) Phaser crystallographic software. *J Appl Crystallogr* **40**, 658–674.
- 14 45. Langer G, Cohen SX, Lamzin VS & Perrakis A (2008) Automated macromolecular  
15 model building for X-ray crystallography using ARP/ wARP version 7. *Nat Protoc* **3**,  
16 1171–1179.
- 17 46. Emsley P, Lohkamp B, Scott WG & Cowtan K (2010) Features and development of  
18 Coot. *Acta Crystallogr D Biol Crystallogr* **66**, 486–501.
- 19 47. Afonine PV, Grosse-Kunstleve RW, Echols N, Headd JJ, Moriarty NW,  
20 Mustyakimov M, Terwilliger TC, Urzhumtsev A, Zwart PH & Adams PD (2012)  
21 Towards automated crystallographic structure refinement with phenix.refine. *Acta*  
22 *Crystallogr D Biol Crystallogr* **68**, 352–367.
- 23 48. Chen VB, Arendall III WB, Headd JJ, Keedy DA, Immormino RM, Kapral GJ,  
24 Murray LW, Richardson JS & Richardson DC (2010) MolProbity: all-atom structure  
25 validation for macromolecular crystallography. *Acta Crystallogr D Biol Crystallogr* **66**,  
26 12–21.
- 27 49. Abagyan RA, Totrov MM & Kuznetsov DA (1994) ICM: A new method for protein  
28 modeling and design: applications to docking and structure prediction from the distorted

1 native conformation. *J Comp Chem* **15**, 488–506.

2

3 **Supporting information**

4 Additional supporting information may be found in the online version of this article at  
5 the publisher's web site:

6 Table S1. Primers sequences for loop exchange mutants



Table 1 Kinetic parameters of mannanases

Enzyme	Substrate	$k_{\text{cat}}$ $\text{s}^{-1}$	Relative $k_{\text{cat}}$	$K_{\text{m}}$ mM	Relative $K_{\text{m}}$	$k_{\text{cat}}/K_{\text{m}}$ $\text{s}^{-1} \cdot \text{mM}^{-1}$	Relative $k_{\text{cat}}/K_{\text{m}}$
StMandC	GGM5	$7.0 \times 10^{-3} \pm 4.0 \times 10^{-4}$	1.0	$7.61 \pm 1.44$	1.0	$9.2 \times 10^{-4}$	1.0
	M4	$1.3 \pm 4.7 \times 10^{-2}$	1.0	$3.13 \pm 0.25$	1.0	$4.2 \times 10^{-1}$	1.0
	M5	$3.7 \pm 5.7 \times 10^{-1}$	1.0	$1.15 \pm 0.36$	1.0	3.2	1.0
	M6	$2.8 \pm 6.2$	1.0	$1.01 \pm 0.46$	1.0	28	1.0
TfMandC	GGM5	$8.2 \times 10^{-4} \pm 1.0 \times 10^{-4}$	0.1	$12.0 \pm 4.0$	1.6	$6.8 \times 10^{-5}$	0.07
	M4	$7.4 \times 10^{-1} \pm 4.8 \times 10^{-2}$	0.6	$1.09 \pm 0.21$	0.3	$6.8 \times 10^{-1}$	1.6
	M5	$48.1 \pm 3.3$	13.2	$1.02 \pm 0.17$	0.9	47	12.7
	M6	$60 \pm 11$	2.1	$0.88 \pm 0.36$	0.9	68	2.4
StW281AdC	GGM5	$4.8 \times 10^{-3} \pm 3.0 \times 10^{-4}$	0.7	$9.08 \pm 1.97$	1.2	$5.3 \times 10^{-4}$	0.6
	M4	$2.9 \times 10^{-1} \pm 3.7 \times 10^{-2}$	0.2	$4.50 \pm 1.10$	1.4	$6.3 \times 10^{-2}$	0.2
	M5	$4.2 \pm 9.0 \times 10^{-1}$	1.1	$2.58 \pm 1.00$	2.2	1.6	0.4
	M6	$20.1 \pm 5.2$	0.7	$1.62 \pm 0.37$	1.6	12	0.4
StD310AdC	GGM5	$2.3 \times 10^{-3} \pm 2.0 \times 10^{-4}$	0.3	$10.3 \pm 2.9$	1.4	$2.3 \times 10^{-4}$	0.2
	M4	$1.5 \pm 1.7 \times 10^{-1}$	1.1	$2.97 \pm 0.79$	0.7	$5.0 \times 10^{-1}$	1.2
	M5	$4.7 \pm 4.7 \times 10^{-1}$	1.3	$1.19 \pm 0.32$	1.0	3.9	1.1
	M6	$30.2 \pm 3.2$	1.1	$1.34 \pm 0.27$	1.3	22	0.8

The relative  $k_{\text{cat}}$ ,  $K_{\text{m}}$ , and  $k_{\text{cat}}/K_{\text{m}}$  values of StMandC were 1.0 toward each substrate.

Table 2 Data collection and refinement statistics

	StMandC	StE273AdC
Space group	$P2_12_12_1$	$P2_12_12_1$
Unit cell parameters ( $a, b, c$ ; Å)	65.86, 100.85, 105.24	65.71, 100.71, 104.74
Resolution range (Å)	50–1.6 (1.7–1.6)	50–1.50 (1.59–1.50)
No. of unique reflections	90737 (14792)	109438 (15735)
$R_{\text{meas}}$	0.202 (0.913)	0.106 (0.587)
Completeness (%)	97.5 (99.3)	98.0 (88.2)
$\langle I/\sigma(I) \rangle$	9.96 (2.25)	13.11 (2.53)
Multiplicity	5.1 (4.9)	4.7 (3.5)
Refinement		
$R_{\text{work}}$	0.1601	0.1458
$R_{\text{free}}$	0.1938	0.1727
No. of protein atoms	4610	4644
No. of sugar atoms	0	191
No. of glycerol atoms	36	42
No. of water molecules	798	795
No. of ions	4 (Na <sup>+</sup> )	5 (Ca <sup>2+</sup> )
Averaged B-factors (Å <sup>2</sup> )		
Protein	9.6	11.2
Sugar	-	26.4
Glycerol	27.7	24.2
Water	25.4	26.8
Ion	16.6	18.3
r.m.s.d. <sup>a</sup> values from ideal		
Bond lengths (Å)	0.008	0.011
Bond angles (°)	1.188	1.398
Ramachandran plot analysis		
Favored region (%)	96.82	97.36
Allowed region (%)	3.01	2.31
Outlier region (%)	0.17	0.33

<sup>a</sup> r.m.s.d., root mean square deviation.

1

2

1 **Figure legends**

2 Figure 1. GGM5 hydrolysis by StMandC and TfMandC. (A) Schematic representation of  
3 GGM5 hydrolysis by mannanases. The parenthesis and numbers show the minus subsites  
4 in StMandC and TfMandC. The triangles show the cleavage site for StMandC (closed)  
5 and TfMandC (open). (B) HPAEC-PAD analysis of the hydrolysis products. (a) GGM5  
6 and StMandC; (b) GGM5 and TfMandC; and (c) GGM5. (C) HPLC analysis of  
7 GGM5-ABEE hydrolysis products. (a) GGM5-ABEE and StMandC; (b) GGM5-ABEE  
8 and TfMandC; and (c) GGM5-ABEE.

9

10 Figure 2. Evaluation of the region involved in GGM5 hydrolysis activity. (A) Schematic  
11 representation of the structures of the parent and chimeric enzymes. Amino acid numbers  
12 and the length of StMan are shown above and inside the bar, respectively. GGM5  
13 hydrolysis products are shown on the right side of the bar. (B) Alignment of the amino  
14 acid sequences responsible for GGM5 hydrolysis specificity of StMan and TfMan. The  
15 numbers represent each amino acid residue. (C) Schematic representation of the  
16 structures of the loop-substitution mutants. As shown in Fig. 2A, the hydrolysis products  
17 from GGM5 are shown on the right side of each bar. The “N.D.” represents no hydrolysis  
18 products detected.

19

20 Figure 3. HPAEC-PAD analysis of GGM5 hydrolysis products by mutated mannanases.  
21 GGM5 was hydrolyzed by chimeric enzymes (A) and loop-substitution mutants of  
22 StMandC and TfMandC (B).

23

24 Figure 4. Overall structure of StMandC and StE273AdC with M6. (A) The superimposed  
25 structure of StMandC and StE273AdC with M6. The peptide colors (from purple to red)  
26 correspond to the N-terminus to the C-terminus. L1-L8 in the figure shows the loop  
27 structures from loop1 to loop8, respectively. Mannose residues are shown as yellow and  
28 green sticks. (B) A superimposed structure of StMandC and StE273AdC. Amino acid

1 residues for mutagenesis in this study are shown. White and blue sticks indicate  
2 StMandC (free form) and StE273AdC (complex with substrate), respectively. (C)  
3 Mannose structure at subsites -2 to +1. Mannobiose at subsites -2 and -1 is shown by a  
4 green stick. Mannobiose at subsites -1 and +1 which distorted the mannose structure at  
5 subsite -1 is shown as a yellow stick. (D) Plus subsite binding residues in StMandC and  
6 StE273AdC. White and blue sticks indicate StMandC and StE273AdC, respectively. The  
7 numbers in the figure indicate subsites.  $\sigma_A$ -weighted  $F_o-F_c$  omit map is contoured at  $3\sigma$   
8 (C and D).

9  
10 Figure 5. Structural comparison between StE273AdC and *T. fusca* KW3 mannanase  
11 (PDB code: **1BQC** and **3MAN**). The minus and plus subsites were compared (A)  
12 between StE273AdC and 3MAN, and (B) between StE273AdC and 1BQC, respectively.  
13 Green and dark blue sticks indicate StE273AdC and TfMandC. Amino acid residues of  
14 StE273AdC, which are related to substrate-binding, are shown in the figure, except for  
15 Val263 of 3MAN. Mannose residues from StE273AdC and 3MAN are shown as yellow  
16 and gray sticks. The numbers in the panels indicate the subsites.

17  
18 Figure 6. Surface view and superimposed model of StE273AdC with *T. fusca* KW3  
19 mannanase (PDB code: **1BQC**). Surface view of the superimposed model of StMandC  
20 (green) and 1BQC (orange) (A), StMandC (B), and 1BQC (C) from the upper (left panel)  
21 and side clefts from the reducing terminus (right panel). Mannose residues from  
22 StE273AdC are shown as a stick structure. The numbers in the figure indicate the  
23 subsites.

24  
25 Figure 7. Hydrolysis products of M5 by StMandC and TfMandC. Hydrolysis products of  
26 M5 by StMandC and TfMandC were analyzed by HPAEC-PAD. Hydrolysis products  
27 were separated by an isocratic flow of 200 mM NaOH.

28

1 Figure 8. Primary structure alignment of bacterial mannanases. Alignment focused on  
2 loop7 and loop8 of bacterial mannanase: (A) similar to StMan and (B) similar to TfMan.  
3 The amino acid sequences (A) of StMan from *Streptomyces thermolilacinus*  
4 (BAK26781); WP\_023591108, *Streptomyces violaceusniger* mannan  
5 endo-1,4- $\beta$ -mannosidase; YP\_004802777, *Streptomyces* sp. SirexAA-E  
6 cellulose-binding family protein; CAJ88324, *Streptomyces ambofaciens* ATCC 23877  
7 putative secreted  $\beta$ -mannosidase; WP\_018555858, *Streptomyces* sp. ATeXAB-D23  
8 beta-mannosidase; NP\_733506, *Streptomyces coelicolor* A3(2)  $\beta$ -mannosidase;  
9 WP\_005475300, *Streptomyces bottropensis* glycosylhydrolase; YP\_003493383,  
10 *Streptomyces scabiei* 87.22 putative secreted glycosyl hydrolase; YP\_007859663,  
11 *Streptomyces* sp. PAMC26508 putative secreted  $\beta$ -mannosidase; YP\_004924956,  
12 *Streptomyces flavogriseus* ATCC 33331 glycoside hydrolase 5; WP\_004003745,  
13 *Streptomyces viridochromogenes* Tue57 putative Secreted  $\beta$ -mannosidase;  
14 WP\_020123328, *Streptomyces canus*  $\beta$ -mannosidase; WP\_020140407, *Streptomyces* sp.  
15 351MFTsu5.1  $\beta$ -mannosidase. The amino acid sequence (B) of TfMan from  
16 *Thermobifida fusca* (AAZ54938); StManII from *Streptomyces thermoluteus*  
17 (BAM62868); SlMan from *Streptomyces lividans* 1326 (AAA26710); ADK91085,  
18 *Streptomyces* sp. S27  $\beta$ -1,4-mannanase; WP\_005474921, *Streptomyces bottropensis*  
19 glycosylhydrolase; CAA20610, *Streptomyces coelicolor* A3(2)  $\beta$ -mannosidase;  
20 CBG75158, *Streptomyces scabiei* 87.22 putative secreted glycosyl hydrolase; CCA60191,  
21 *Streptomyces venezuelae* ATCC 10712 Endo-1,4- $\beta$ -xylanase A precursor; CCA60180,  
22 *Streptomyces venezuelae* ATCC 10712 Endo-1,4- $\beta$ -xylanase A precursor;  
23 YP\_008735110, *Actinoplanes friuliensis* DSM 7358 putative glycosyl hydrolase;  
24 YP\_007953378, *Actinoplanes* sp. N902-109 secreted  $\beta$ -mannosidase; WP\_020640659,  
25 *Amycolatopsis balhimycina*  $\beta$ -mannosidase; YP\_003637895, *Cellulomonas flavigena*  
26 DSM 20109 glycoside hydrolase family protein; YP\_004081647, *Micromonospora* sp.  
27 L5  $\beta$ -mannanase-like protein ; WP\_018788190, *Micromonospora* sp. CNB394 mannan  
28 endo-1,4- $\beta$ -mannosidase; YP\_004404351, *Verrucospora maris* AB-18-032 glycoside

1 hydrolase family protein. The conserved regions and gaps are indicated by highlight and  
2 (-), respectively. The number of the alignment is indicated by the amino acid residues of  
3 each protein. “\*1” shows the species possessed more than two kinds of GH5 mannanase  
4 genes: NP\_733506 and WP\_005474921 from *S. coelicolor* A3(2); YP\_003493383 and  
5 CBG75158 from *S. scabiei* 87.22; WP\_005475300 and WP\_005474921 from *S.*  
6 *bottropensis*. “\*2” shows the species possessed GH26 mannanase gene in addition to  
7 GH5 mannanase gene.

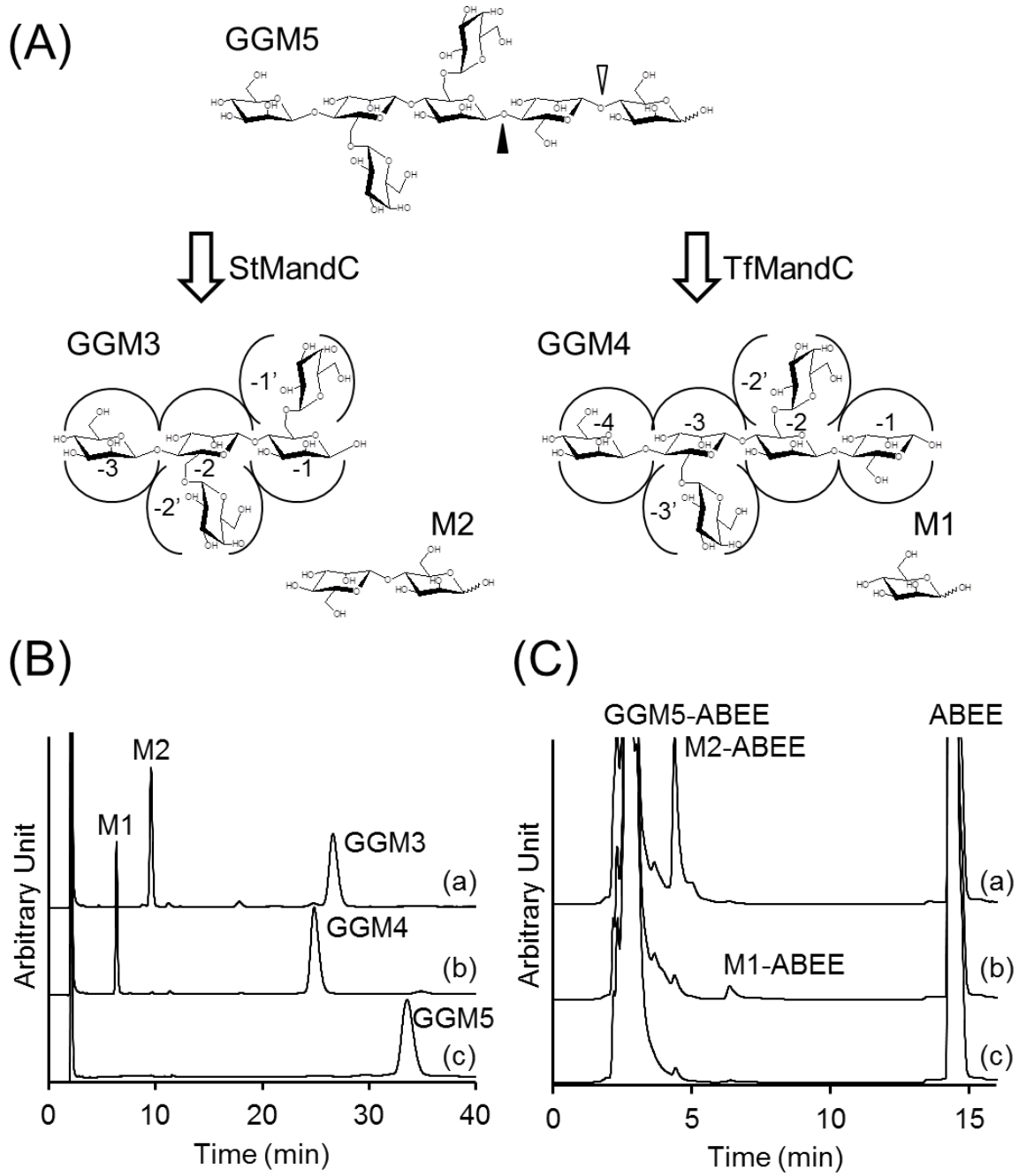


Figure 1 Kumagai et al

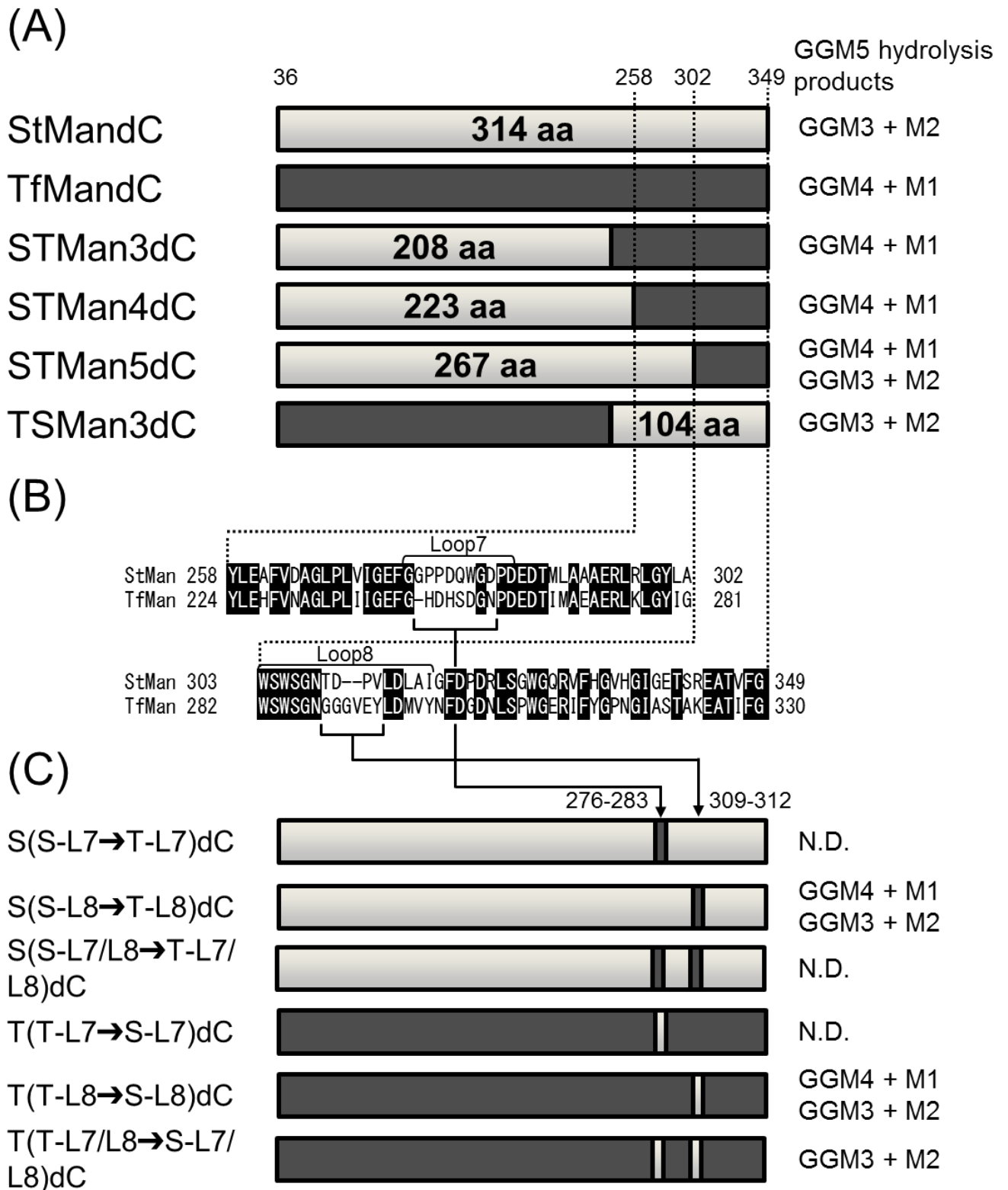


Figure 2 Kumagai et al



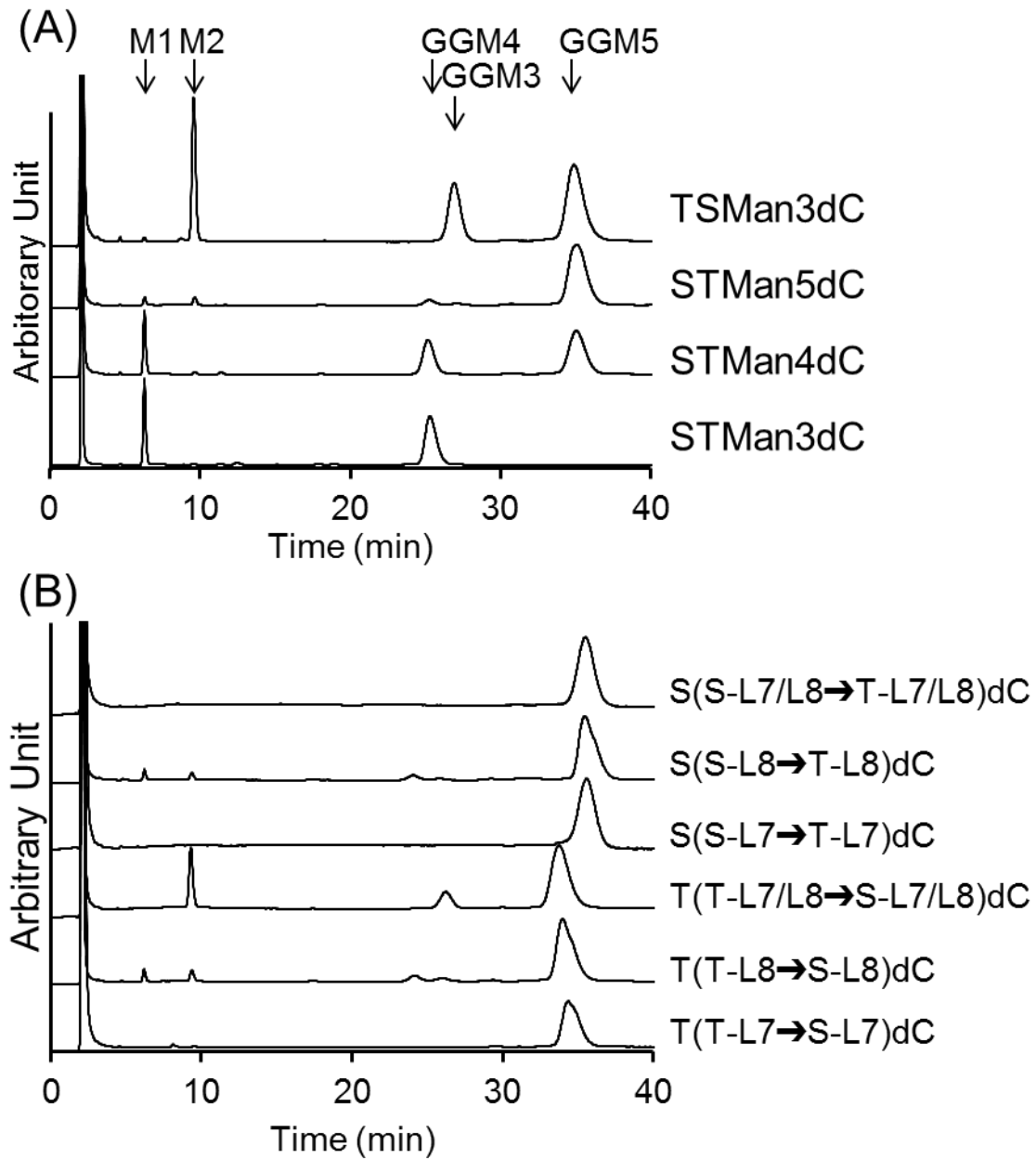


Figure 3 Kumagai et al

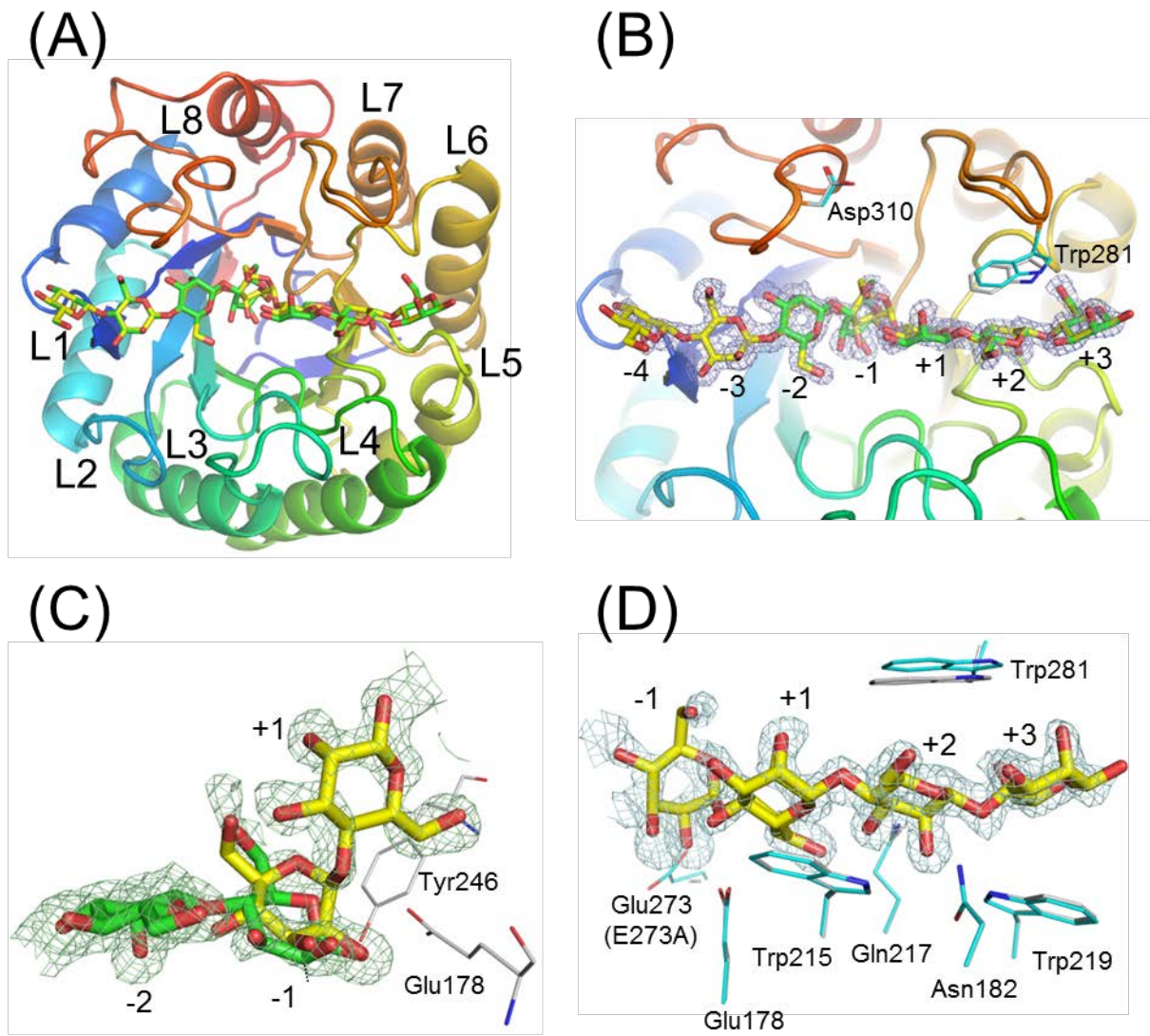
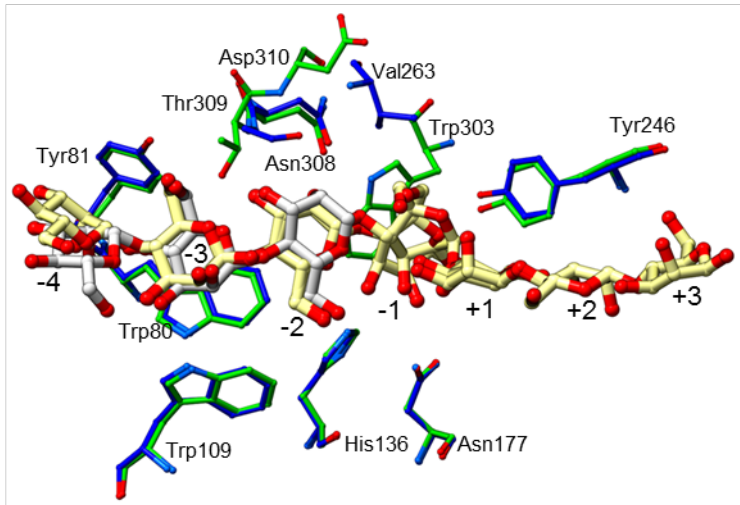


Figure 4 Kumagai et al

**(A) StE273AdC + 3MAN**



**(B) StE273AdC + 1BQC**

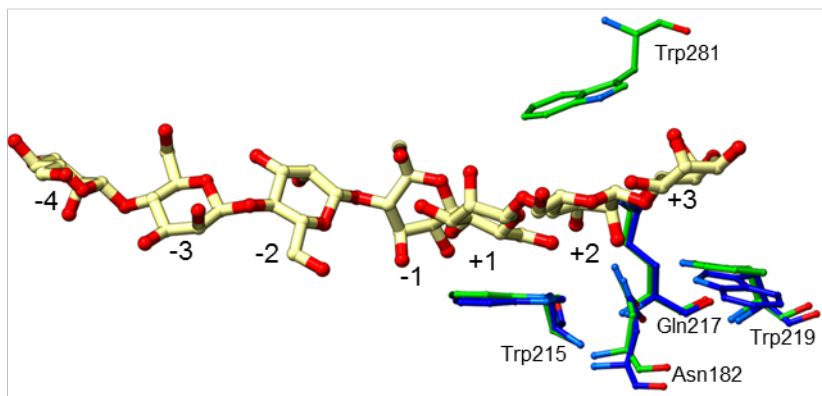
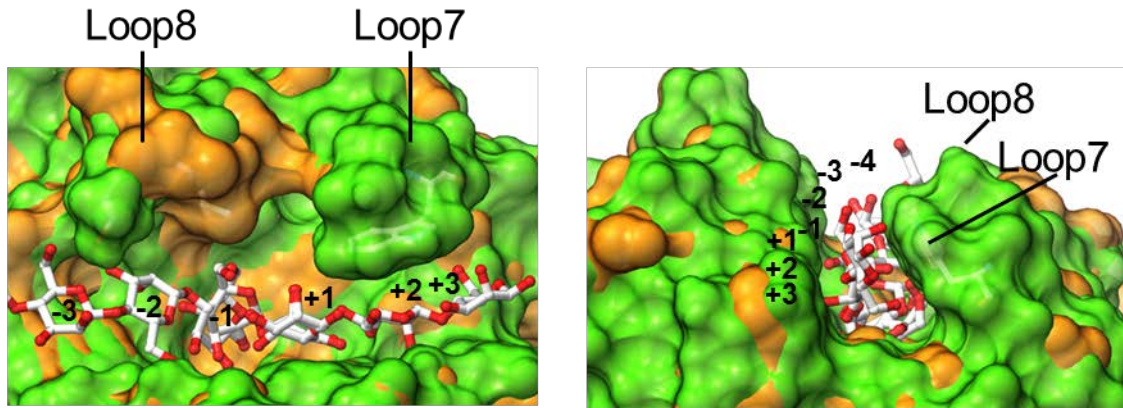
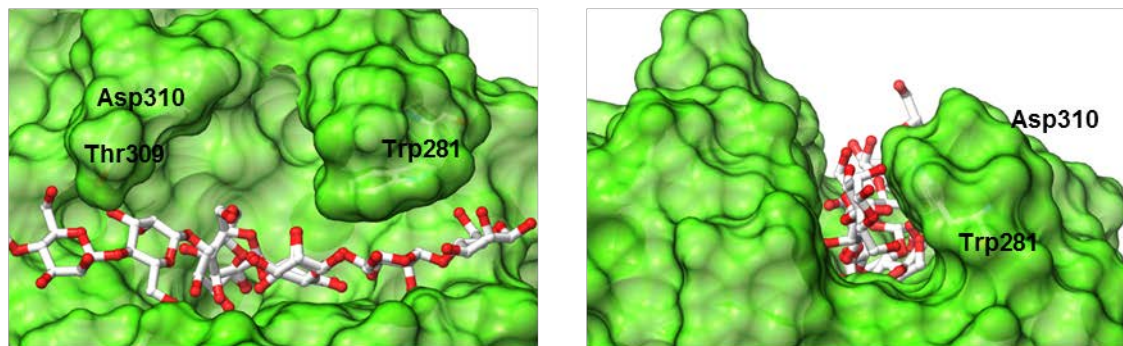


Figure 5 Kumagai et al

(A) StE273AdC + 1BQC



(B) StE273AdC



(C) 1BQC

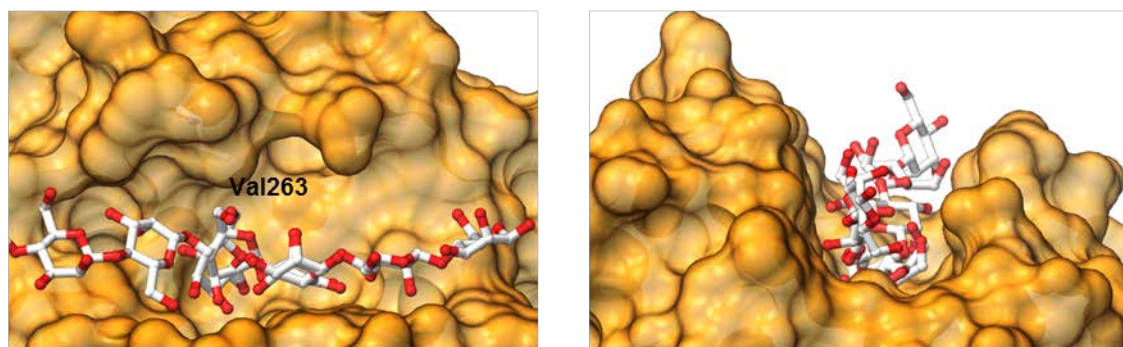


Figure 6 Kumagai et al

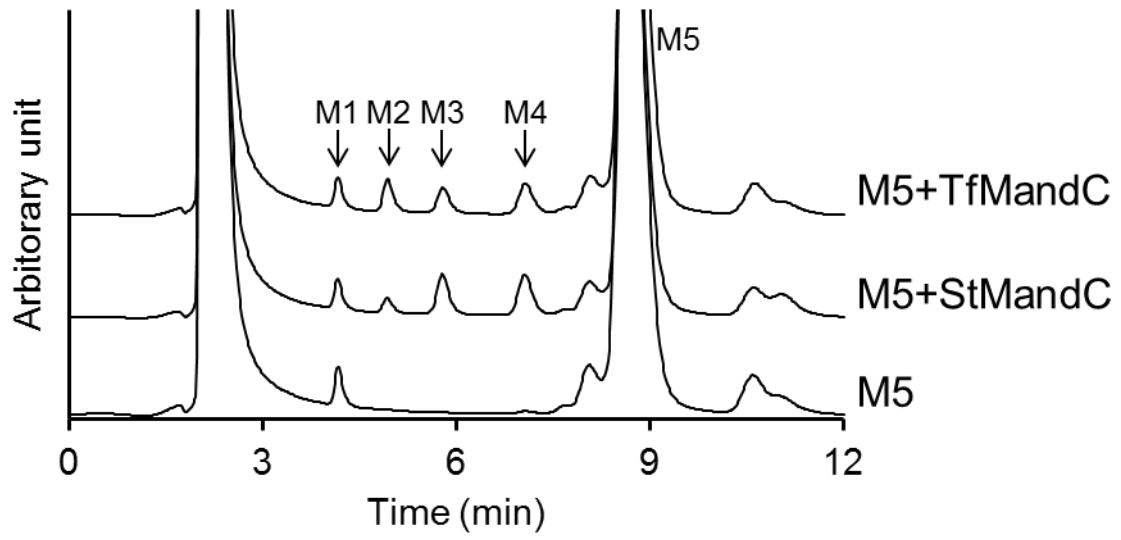


Figure 7 Kumagai et al

1

		Loop-7	Loop-8	
(A)	StMan	271	I G E F G G P P D C W G D P D E D T M L A A A E R L R L G Y L A W S W S G N — T D P V L D L A I G	318
	WP_023591108	271	I G E F G G P P D C W G D P D E D T M L A A A E R L R L G Y L A W S W S G N — T D P V L D L A I G	318
	YP_004802777	271	I G E F G G P A D C Y G D P D E D T M M A T A E E L G L G Y L A W S W S G N — T D P V L D L V L D	318
	CAJ88324	267	I G E F G G P A D C W G D P D E D T M M A A A E R L D L G Y L A W S W S G N — T D P V L D L A I D	314
	WP_018555858	261	I G E F G G P A D C Y G D P D E D T M M A D A E Q L G L G W I A W S W S G N — T D P V L D L A I D	308
	NP_733506 *1	267	I G E F G G P A D C Y G D P D E D T M M A T A E Q L R L G Y L A W S W S G N — T D P V L D L A L D	314
	WP_005475300 *1	267	I G E F G G P A D C W G D P D E D T M M A A A E Q L D L G Y L A W S W S G N — T D P V L D L S I G	314
	YP_003493383 *1,2	267	I G E F G G P A D C W G D P D E D T M M A A A E R L D L G Y L A W S W S G N — T D P V L D L S I G	314
	YP_007859663 *2	268	I G E F G G P A D C W G D P D E D T M M A T A E Q L D L G Y L A W S W S G N — T D P I L D L A I D	315
	YP_004924956 *2	249	I G E F G G P A D C W G D P D E D T M M A T A E Q L D L G Y L A W S W S G N — T D P I L D L A I D	296
	WP_004003745 *2	246	I G E F G G P P D C W G D P D E D T M M A A A Q Q L K L G Y L A W S W S G N — T D P I L D L A I D	293
	WP_020123328 *2	240	I G E F G G P A D C W G D P D E D T M M A T A E Q L H L G Y L A W S W S G N — T D T I L D L V L D	287
	WP_020140407 *2	241	I G E F G G P A D C W G D P D E D T M M A T A Q R L G L G Y L A W S W S G N — T D P S L D L V L G	288
(B)	TfMan	251	I G E F G — H D H S D G N P D E D T I M A E A E R L K L G Y I G W S W S G N G G G V E Y L D M V Y N	299
	StMan II	246	V G E F G — H D H S D G N P D E D A I L S V T R Q L G I G Y L G W S W S G N G G G V E Y L D M V E N	304
	SIMan	257	V G E F G — D C H S D G N P D E D A I M A T A Q S L G V G Y L G W S W S G N G G G V E Y L D M V N G	305
	ADK91085	259	V G E F G — H N H G D G P D E N A I M A T A Q S L R V G Y L G W S W S G N G G G V E Y L D M V N G	307
	WP_005474921 *1	261	V G E F G — H D H S D G N P D E D A I L A T A Q R L G L G Y L G W S W S G N G G G V E Y L D M V T G	309
	CAA20610 *1	258	V G E F G — D C H S D G N P D E D A I M A T A Q S L G V G Y L G W S W S G N G G G V E Y L D M V N G	306
	CBG75158 *1, 2	333	I G E F G — H E H S D G N P D E D A I L A A A Q R L G L G Y L G W S W S G N G G G V E Y L D L V T G	381
	CGA60191 *2	258	V G E F G — D N H S D G N P D E N A I M A T T Q S L R V G Y L G W S W S G N G S G V E Y L D M V T G	306
	CCA60180 *2	253	V G E F G — Y D H S D G N P D E D A I M A T A R R L D L G Y M G W S W S G N G G G V E Y L D L A T G	301
	YP_008735110 *2	251	V G E F G — H N H S D G N P D E D T I L A T A Q A Q G I G Y L G W S W S G N G G G V E Y L D L V T N	299
	YP_007953378 *2	244	V G E F G — F D H S D G N P D E D T I M A T A Q R L G I G Y L G W S W S G N G G G V E Y L D M V T G	292
	WP_020640659 *2	462	V G E F G — N M H T D G N P D E D T I M A Q A Q A R G L G Y L G W S W S G N S S D V A Y L D M T N N	510
	YP_003637895 *2	256	I G E F G — I D H S D G P D E A T I M R E A T E R G I G Y Y G W S W S G N S G G V E Y L D M V T G	305
	YP_004081647 *2	249	V G E F G — F N H S D G N P D E D A I M A Y A Q A N G I G Y L G W S W S G N G G G V E Y L D M T T A	297
	WP_018788190 *2	249	V G E F G — F N H S D G N P D E D A I M A Y A Q A N G I G Y L G W S W S G N G G G V E Y L D M T T G	297
	YP_004404351 *2	249	V G E F G — H Y H S D G P D E D A I L S Y T Q A N G I G W L G W S W S G N G G G V E Y L D M A T N	297

Figure 8 Kumagai et al

1

2

Table S1. Primers sequences for loop exchange mutants

Primer	Restriction site	Sequence <sup>a</sup>
StFw	<i>NdeI</i>	5'- <u>CATATG</u> CGGACCGCCCCGCCCCG-3'
StL7Re1	<i>EcoRI</i>	5'- <u>GAATTC</u> CCCCGATGACCAGCGGCAGC-3'
StL7Fw1		5'-CACGACCACTCCGACGGCAACCCGGACGAGGACACGATGC-3'
StL7Fw2	<i>EcoRI</i>	5'-CCC <u>GAATTC</u> CACGACCACTCCGACGGCAACC-3'
StL8Re1		5'-AGGTACTCGACCCCGCCGCGTGTGCCGCTCCACGACCAGG-3'
StL8Re2	<i>BglII</i>	5'-TTC <u>AGATCT</u> AGGTACTCGACCCCGCCGCGTGTGC-3'
StL8Fw1		5'-ACGGCGGGCGGGTTCGAGTACCTCGACCTGGCGATCGGGTT-3'
StL8Fw2	<i>BglII</i>	5'-AAT <u>AGATCT</u> TGGCGATCGGGTTCGACCCCGAC-3'
StCDRe	<i>HindIII</i>	5'- <u>AAGCTT</u> TTCAGGTGTCGCCGGGGTTTCCCC-3'
TfFw	<i>NdeI</i>	5'- <u>CATATG</u> GCCACCGGGCTCCACGTCAAG-3'
TfL7Re1	<i>EcoRI</i>	5'- <u>GAATTC</u> GCCGATGATGAGCGGCAGG-3'
TfL7Fw1		5'-CGCCCGACCAGTGGGGCGACCCCGACGAGGACACGATCAT-3'
TfL7Fw2	<i>EcoRI</i>	5'-AGG <u>GAATTC</u> GCGGGGCCCGCCCGACCAGTGGGGCG-3'
TfL8Re1		5'-ATGTCGAGGACGGGGTTCGGTGTGTGCCGCTCCACGACCAGC-3'
TfL8Re2	<i>BglII</i>	5'- <u>CAGATCT</u> AGGACGGGGTTCGGTGTGTCCCG-3'
TfL8Fw1		5'-GCGGCAACACCGACCCCGTCCTCGACATGGTGTACAACCTT-3'
TfL8Fw2	<i>BglII</i>	5'-AAT <u>AGATCT</u> TGTGTACAACCTTCGACGGCGAC-3'
TfCDRe	<i>HindIII</i>	5'- <u>AAGCTT</u> TTCACGGGCCCGGCTGGGAGCC-3'

<sup>a</sup>Underline shows the restriction site